Protocol
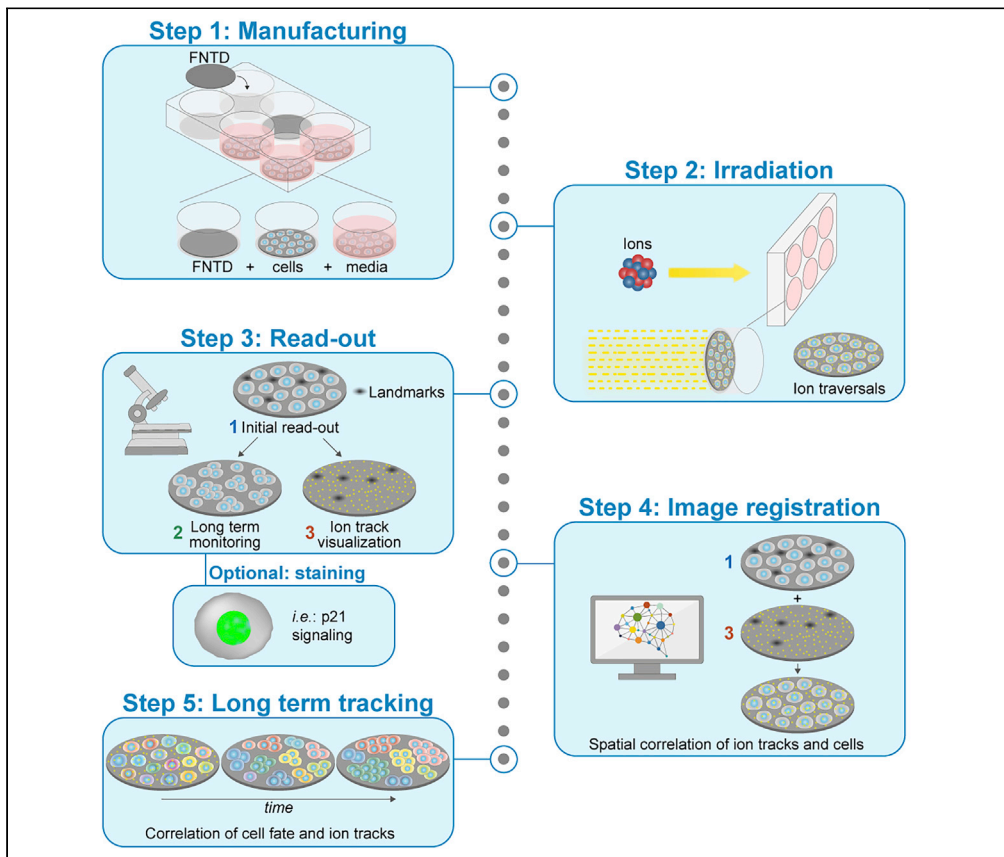
Biosensor Cell-Fit-HD^{4D} for correlation of single-cell fate and microscale energy deposition in complex ion beams

Julian Schlegel, Hans Liew, Katrin Rein, Oleh Dzyubachyk, Jürgen Debus, Amir Abdollahi, Martin Niklas

j.schlegel@dkfz.de (J.S.)
m.niklas@dkfz.de (M.N.)

Highlights

Cell-Fit-HD^{4D} is an *in vitro* biosensor for clinical ion beams

Cell-Fit-HD^{4D} combines single-cell dosimetry with individual tracking of tumor cells

Cell-Fit-HD^{4D} visualizes variability in radiation response in tumor cell population

We present a protocol for the biosensor Cell-Fit-HD^{4D}. It enables long-term monitoring and correlation of single-cell fate with subcellular-deposited energy of ionizing radiation. Cell fate tracking using widefield time-lapse microscopy is uncoupled in time from confocal ion track imaging. Registration of both image acquisition steps allows precise ion track assignment to cells and correlation with cellular readouts.

Publisher's note: Undertaking any experimental protocol requires adherence to local institutional guidelines for laboratory safety and ethics.

Protocol

Biosensor Cell-Fit-HD[4D] for correlation of single-cell fate and microscale energy deposition in complex ion beams

Julian Schlegel,[1,2,5,6,*] Hans Liew,[1,2] Katrin Rein,[1,2] Oleh Dzyubachyk,[3] Jürgen Debus,[1,2,4] Amir Abdollahi,[1,2,4] and Martin Niklas[1,2,5,*]

[1]Division of Molecular and Translational Radiation Oncology and Clinical Cooperation Unit Translational Radiation Oncology, German Cancer Research Center (DKFZ) and Heidelberg University Hospital, 69120 Heidelberg, Germany

[2]National Center for Tumor Diseases, German Cancer Consortium, Heidelberg Institute of Radiation Oncology and National Center for Radiation Oncology, 69120 Heidelberg, Germany

[3]Department of Radiology and Department of Cell and Chemical Biology, Leiden University Medical Center, 2333 ZC Leiden, the Netherlands

[4]Heidelberg Ion-Beam Therapy Center (HIT), 69120 Heidelberg, Germany

[5]Technical contact

[6]Lead contact

*Correspondence: j.schlegel@dkfz.de (J.S.), m.niklas@dkfz.de (M.N.)
https://doi.org/10.1016/j.xpro.2022.101798

SUMMARY

We present a protocol for the biosensor Cell-Fit-HD[4D]. It enables long-term monitoring and correlation of single-cell fate with subcellular-deposited energy of ionizing radiation. Cell fate tracking using widefield time-lapse microscopy is uncoupled in time from confocal ion track imaging. Registration of both image acquisition steps allows precise ion track assignment to cells and correlation with cellular readouts.

For complete details on the use and execution of this protocol, please refer to Niklas et al. (2022).

BEFORE YOU BEGIN

The protocol below describes the construction and application of the cell-fluorescent ion track hybrid detector 4D (Cell-Fit-HD[4D]). This biosensor is based on a fluorescent nuclear track detector (FNTD) covered with a viable cell layer. The protocol extends the previously presented biosensor Cell-Fit-HD for static measurements in physical energy deposition and biological response in ion beam irradiation (Niklas et al., 2013b).

Before starting, we recommend the general considerations for the biosensor and the associated experiment:

1. General concept.

The seeding and attachment of cells on the fluorescent nuclear track detector (FNTD) allows for visualization and determination of single ions which traverse a cell during irradiation and thus confers microscale dose calculation (Akselrod and Sykora, 2011; Greilich et al., 2013; Klimpki et al., 2016). This application was previously utilized for the static correlation of ion hits with inflicted DNA damage in cells which were directly fixed following irradiation (Kodaira et al., 2015; Niklas et al., 2013b), as well as correlation with real time double strand breaks emergence in living cells (McFadden et al., 2020). The biosensor Cell-Fit-HD[4D] and associated protocol presented here, enable the combination of cellular energy deposition analysis and cell fate tracking for several days. This is

primarily achieved by time-wise decoupling of widefield live cell microscopy and confocal readout of the FNTD, which is conducted after cell imaging and fixation. Cell-Fit-HD^{4D} comprises two distinct architectures, both of which fulfill the requirements for cell homeostasis and imaging, but differ in their focus on simplicity and light channel availability.

2. Choice of architecture.

In case of the wafer architecture, cells (biological compartment) are directly attached to a thin, FNTD wafer (physical compartment), which substantially facilitates the post-imaging ion track registration procedure. However, the light beam of an inverted widefield microscope needs to pass the FNTD wafer during cell imaging, which impairs signal-to-noise ratio (SNR) and restricts cell imaging to the red spectrum due to FNTD emission spectrum. This can be circumvented by inversion of the biosensor by mounting a FNTD in small distance on top of the cells. However, in this setup - the mounting architecture - the FNTD is later anew positioned for ion track readout. Hence, the initially imaged positions need to be re-identified. This protocol specifically outlines the application of the biosensor using the wafer architecture. Detailed information on the mounting architecture can be found in (Niklas et al., 2022). Here, we describe the tracking of A549 proliferation dynamics and DSB dynamics.

In contrast to previously presented in-beam live-cell microscopy in combination with the FNTD (McFadden et al., 2020), Cell-Fit-HD^{4D} is transferred to a standard widefield microscope with a respective incubator and initially imaged within a few minutes post-irradiation – sufficient to yield and correlate relevant immediate molecular responses like formation of radiation induced DNA damage foci (RIF).

3. Consideration of Imaging parameters.

The choice of imaging system and parameters is not limited, except for excitation light channel availability when using the wafer architecture in combination with widefield microscopy. Application of a confocal system for cell imaging on the FNTD re-extends the susceptible spectrum at the cost of cell viability and/ or acquirable frame number. Ultraviolet laser excitation ($\sim$ 405 nm) prior to ion track visualization should be avoided due to FNTD color center activation. The total imaging timespan is mainly restricted by the increasing cellular density which negatively affects automatic cell tracking performance. Thus, maximum live-cell imaging duration is majorly determined by cell proliferation rate and initial seeding density and should be adjusted and optimized for each cell line specifically.

4. Post-processing and analysis.

Once live cell microscopy is completed, the imaged cells can be utilized for standard cell culture or analysis procedures like trypsinization, fixation, or lysis. The presence of cells is not required for FNTD readout and correlation with ion tracks as the initially acquired images (the so-called initial readout) are used for ion track–cell–correlations. Here we exemplary outline the fixation, endpoint-staining and static endpoint-imaging of cells attached to the FNTD.

KEY RESOURCES TABLE

REAGENT or RESOURCE	SOURCE	IDENTIFIER
Antibodies		
Mouse p21 Waf1/Cip1/CDKN1A (F-5) dilution 1:50	Santa Cruz	Cat#sc-6246; RRID: AB_628073
Rabbit p53 binding protein 1 (53BP1) dilution 1:200	Cell Signaling Technology	Cat#4937; RRID: AB_10694558
Mouse Anti-Phospho-Histone H2A.X (Ser 139) dilution 1:100	Cell Biolabs	Cat#STA-321

(Continued on next page)

Continued

REAGENT or RESOURCE	SOURCE	IDENTIFIER
Goat Anti- Mouse Alexa488 dilution 1;400	Invitrogen	A-11029
Goat Anti- Mouse Alexa647 dilution 1;400	Invitrogen	Invitrogen
Bacterial and virus strains		
Retro-X Universal Packaging System	Takara	Cat# 631530
Chemicals, peptides, and recombinant proteins		
Ethanol 100%		
Bovine Serum albumin (BSA)		
4′,6-Diamidino-2-phenylindol (DAPI)	Thermo Fisher Scientific	Cat# D1306
L-Glutamine (200 mM)	Thermo Fisher Scientific	A2916801
Triton-X 100		
Experimental models: Cell lines		
Human: A549 lung carcinoma cells	ATCC	Cat#CCL-185; RRID:CVCL_0023
Recombinant DNA		
mCherry-BP1-2 pLPC-PuroApple-53BP1trunc	Addgene	Plasmid #19835 69531 (Dimitrova et al., 2008)
Software and algorithms		
ImageJ		https://imagej.nih.gov/ij/
MatLab	MathWorks https://de.mathworks.com/products/matlab.html	
Level-set based CellTracker	Dzyubachyk et al. (2010)	https://doi.org/10.1109/TMI.2009.2038693
RStudio	RStudio Team, 2020 https://www.rstudio.com/products/rstudio/	
Code applied for data generation reported here	*This paper*	https://doi.org/10.17632/cdt269pw7m.1 https://doi.org/10.17632/
Other		
Fluorescent Nuclear Track Detector (FNTD)	LANDAUER Inc	
6-well imaging plates	MatTek	Cat#P06G-1.5-10-F
Histoacryl® tissue glue	Braun	9381104
wax-polyolefin film	Bemis	HS234526C
Dulbecco's phosphate buffer saline (DPBS)	PAN-Biotech	Cat#P04-53500
Dulbecco's Modified Eagle Medium (DMEM)	Merck Millipore	Cat#FG0415
DMEM Phenol red-free	Merck Millipore	Cat#F0475
Heat Inactivated Fetal Bovine Serum (FBS)	Merck Millipore	Cat# #S0615
Penicillin/ Streptomycin (10.000 U/mL)	Thermo Fisher Scientific	Cat# 15140

MATERIALS AND EQUIPMENT

Following equipment and components are required for the setup and conduction of a Cell-Fit-HD[4D] experiment.

- Ionizing radiation facility.

The characteristics of the FNTD have to be considered when planning the ion beam qualities. The FNTD is very sensitive to ion irradiation. Its readout allows to detect and to reconstruct single ion traversals with a sub-resolution ($\sim$320 nm) using confocal microscopy and even higher ($\sim$80 nm) using optical nanoscopy (Greilich et al., 2013; Klimpki et al., 2016; Niklas et al., 2017). The diameter of a so-called recorded track spot - the ion's characteristic signature left in the FNTD - is dependent on the ion beam quality and is also determined by the point-spread function of the imaging system: it is less than 1 μm for carbon ion irradiation (Niklas et al., 2013d). The FNTD can detect ions with a linear energy transfer (LET) in Al_2O_3 from 0.5 keV/μm to 61,000 keV/μm and has limitations in resolving ion beam fluences > 5 * 10^7 cm^{-2} (Osinga et al., 2013; Sykora et al., 2008). The detection

efficiency is $\geq$ 99.83% for the entire spectrum of primary ions and fragments at energies found in ion-beam cancer therapy (Osinga et al., 2013). These properties allow the FNTD to resolve and to characterize single ion traversals in a clinical ion beam field.

- S1 sterile hood and cell culture incubator.

Enabling proper sterile cell culture as well as sterile construction and preparation of Cell-Fit-HD[4].

- Fluorescent nuclear track detector (FNTD) in the shape of wafers, 6-well imaging plates.

It is important in the construction of the physical compartment of Cell-Fit-HD[4D] to ensure that the diameter of the wafer meets the diameter of the well bottom of the imaging plates. The thickness of wafer should in principal be compatible with the working distance of the microscope's objective. If the thickness exceeds the working distance, a proper imaging of the cell layer might not be possible. Here, wafer of thickness 100 μm were used meeting the working distance of the 40× oil objective used. Additionally, a thickness of 100 μm enables precise ion track reconstruction into the cell layer of < 10 μm thickness.

- Widefield and confocal laser scanning microscope (CLSM).

On the one hand, the widefield microscope requires equipment for live cell microscopy including temperature and atmosphere control for imaging of the cell layer. On the other hand, the equipment of the CLSM requires specific characteristics to readout the FNTD, i.e., physical compartment of Cell-Fit-HD[4D], namely a laser line in the region of 620 nm and an avalanche photodiode (APD) or equivalent. For detailed information on the readout of FNTD we refer to (Greilich et al., 2013; Niklas et al., 2016; Akselrod and Kouwenberg, 2018).

- General lab and cell culture equipment.

Pipettes, Trypsin, cell medium, PBS for cell culture. Forceps for construction of the Cell-Fit-HD[4D] physical compartment and general handling of the FNTD. Such equipment does not underlie specific requirements and might be chosen as available or required based on individual needs.

Prior to Cell-Fit-HD[4D] construction, cells are cultured and potentially transfected with stably expressed fluorescent markers. FNTDs can be cleaned from potential residual lubricant by waterbath sonication. Irradiation plans and setups should be tested in advance.

Full culture medium

Reagent	Final concentration	Amount
DMEM	90%	500 mL
FBS	9%	50 mL
Penicillin/Streptomycin	0.9%	5 mL
Total	N/A	555 mL

Store at 4°C up to 3 months.

Live-cell imaging medium

Reagent	Final concentration	Amount
DMEM Phenol red-free	89%	500 mL
FBS	8.9%	50 mL
Penicillin/Streptomycin	0.9%	5 mL
L-Glutamine	0.9%	5 mL
Total	N/A	560 mL

Store at 4°C up to 3 months.

Blocking buffer		
Reagent	Final concentration	Amount
DPBS	1×	20 mL
BSA	3%	750 µg
Triton-X100 (1% in PBS)	0.2%	5 mL
Total	N/A	25 mL
Store at 4°C up to 1 week.		

STEP-BY-STEP METHOD DETAILS
Construction of Cell-Fit-HD[4D]

⊙ Timing: 15 min to replace glass bottom of a 6-well imaging plate with the FNTD wafer; 5 min dry incubation; overnight incubation to remove potentially residual glue remains and confirm complete sealing.

Timing: 15 min; 4–12 h (overnight) for attachment and morphological inspection for step 2

The Cell-Fit-HD[4D] biosensor combines the physical (FNTD) with the biological (cells) compartment and is optimized for long-term observation of irradiated cells at cell culture conditions.

Note: We would like to refer to the Methods video S1. All steps are performed in a sterile environment of a laminar flow hood. If the CLSM is equipped with a polarized excitation laser beam make sure that the optical axis of the FNTD is in parallel with the polarized excitation laser beam to maximize the readout signal (Greilich et al., 2013).

1. Exchange of glass bottom with FNTD wafer (physical compartment).
   a. Remove the glass bottom of a 6-well plate by applying physical force with a forceps. Ensure complete removal of residual glass and thoroughly clean the adhesive surface from residual glue using 70% EtOH and low-lint laboratory tissues.

Note: A spatial buffer between wells to be irradiated and non-irradiated control-wells is favorable to minimize risk of scatter radiation. The complete plate can be utilized for the experiment.

   b. Apply small drops of tissue glue around the adhesive surface edge of the well using a micro-pipette (take up tissue glue directly from the tube using the pipette). A good estimate for one well are 8 drops of approximately 1 µL in total.
   c. Place the well plate upside down and gently attach the dry FNTD wafer to the well bottom using forceps or a suction contact lens holder.

⚠ CRITICAL: Any glue, even non-visible micro particles of glue within the well causes substantial cytotoxicity. Avoid sidewise movement of the FNTD wafer once attached. Reduce deployed glue volume if necessary.

   d. Incubate the plate upside-down at 37°C in a cell culture incubator for approximately 3 min for the tissue glue to polymerize.
   e. Sterilize the modified wells with 70% EtOH (ethanol) and wash 1× with PBS. Perform these procedures on a tissue paper to directly notice potential leakages.

Note: While leakages might be successfully spot-repaired using additional glue, successful sealing is not guaranteed and can lead to excessive glue within the well. Gently removal of the wafer and restart of the construction protocol might be considered.

f. Fill the modified wells with cell culture medium or PBS and place the plate on several tissue sheets in an incubator at 37°C for a recommended minimum of 6 h–12 h (overnight) to guarantee complete, durable sealing and bind potential glue particles in the fluid.

g. Aspirate the medium.

h. Gently wipe the back side of the FNTD wafer with 70% EtOH. Retrace the marks of the optical axis of the FNTD wafer for later readout.

2. Cell seeding (biological compartment).

Note: In this protocol we describe the cell seeding for A549 cells transduced with a mCherry-TP53BP1 fusion gene (Dimitrova et al., 2008). Yet, several cell lines were previously tested in terms of viability when cultured on the FNTD (Niklas et al., 2013c).

a. Wash, trypsinize, collect and count cells according to standard cell culture procedure.

b. Seed suitable cell numbers in standard medium in the modified wells. A non-modified well with glass bottom might be utilized as a positive control for normal cell physiology.

Note: The seeded cell number directly determines the yielded data points per imaging tile as well as the robustness of automatic cell tracking. For A549 cells, we found 125,000–150,000 cells/ well to present an adequate density for image acquisition up to five days when irradiating with 1 Gy carbon ions.

c. Incubate the Cell-Fit-HD^{4D} plate at room temperature for approximately 20 min to obtain homogenous cell distribution within the well.

d. Incubate under cell culture conditions (37°C, 5% CO_2 for most cell lines) for a minimum of 4 h for cell attachment.

e. Monitor cells using a brightfield microscope (Figure 1).

⚠ CRITICAL: After overnight incubation, disturbed cell homeostasis as a consequence of residual glue should be observable based on abnormal cell morphology. In this case, a successful experimental run of long-term imaging is unlikely.

Setup of imaging program

⏱ Timing: 15 min

Pre-setup of a suitable imaging protocol with appropriate parameters is crucial for immediate imaging start following irradiation as well as for reasonable analysis of biologic readouts.

Note: Optimal image acquisition parameters depend on the observed subject and experimental question. In general, a balance of overall light exposure and imaging duration needs to be found to avoid observation of phototoxicity-related phenomena. The basic protocol for Cell-Fit-HD^{4D} however always consists of the initial readout; the recording of a z-stack which covers the FNTD of ~100 μm in axial dimension as well as the overlying cell layer for later ion track reconstruction, followed by long-term imaging of the cell layer only (Figure 2). In consequence, at least two imaging programs for the very same positions are compiled.

3. Set up initial readout imaging program.

a. Define positions to be scanned based on a 6-well plate dummy or the Cell-Fit-HD^{4D} plate.

Note: The delay between irradiation and the initial stack scan increases with each additional position, which potentially can decrease the precision of single cell energy deposition computation. Ensure that non-irradiated control wells are scanned last.
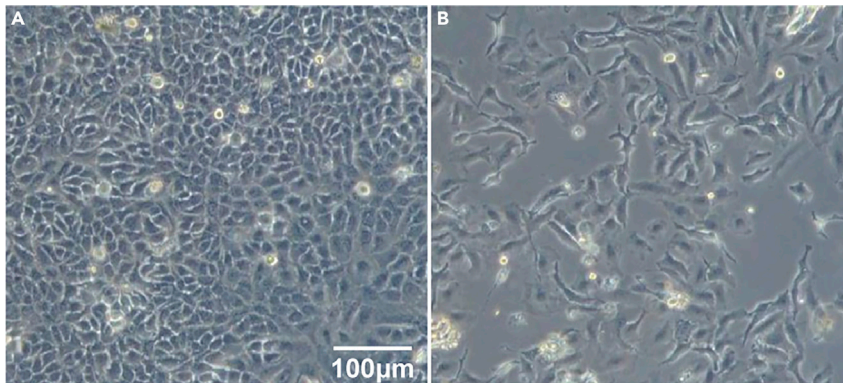
Figure 1. Cell coating of Cell-Fit-HD⁴ᴰ

(A and B) Exemplary comparison of a healthy cell layer (A) and cells showing abnormal morphology as a consequence of suboptimal construction of Cell-Fit-HD⁴ᴰ (B). Images were taken three days after seeding. Residual glue in contact with the medium leads to impaired proliferation as well as enlargement and elongation, indicating physiologic stress. Here, higher cell numbers were seeded for demonstration.

b. Set the z-stack range with intervals of ≤ 3 μm to ensure focused acquisition of the cell layer. The z-range of the initial stack can be set by introduction of an offset based on the autofocus of the cell layer, or via manual determination by use of the actual Cell-Fit-HD⁴ᴰ plate.

c. Select light channels for visualization of the cell layer and determine proper exposure time(s). Select transmitted light channel to visualize the spinels (small and randomly distributed artefacts within the FNTD crystal structure), which will later serve for image registration, best.

Note: The spinels can principally be weakly visualized in the red spectrum, and can be enhanced by image post-processing. Transmitted light exposure should be kept to a minimum, and might be disregarded for long-term imaging due to excess phototoxicity. The exposure time of the cell imaging channel can be lower compared to the time-lapse imaging, as initial imaging only serves segmentation instead of data yield.

d. Set all remaining parameters such as autofocus, image save location etc. according at discretion, and save program.

4. Set up time-lapse imaging program.
   a. Ensure that exactly the same imaging positions are taken over from the initial stack.
   b. Select light channels and determine proper exposure time(s).
   c. Select scanning intervals.

Note: Scanning intervals mostly depend on your experimental question. Distinct scanning intervals might be chosen for different time points. In general, however, a balance needs to be found between phototoxicity (short intervals) and decreasing cell traceability (long intervals). We applied scanning intervals between 15–45 min.

   d. Set all remaining parameters such as autofocus, z-stacks, image save location etc. according at discretion, and save program.
5. Load imaging programs into a successive queue and prepare everything in a way that an instant image acquisition is guaranteed.

Irradiation of Cell-Fit-HD⁴ᴰ

⏱ Timing: 5 min for Cell-Fit-HD⁴ᴰ preparation; 20 min for irradiation setup; 2 min for irradiation (depending on the size of the irradiation field and planned physical dose level).
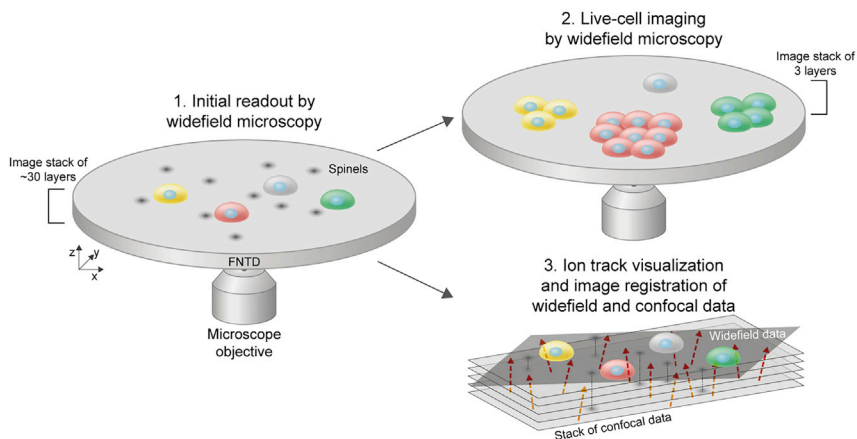
Figure 2. Readout protocol for the biosensor Cell-Fit-HD[4D]

In the initial readout the so-called *initial stack*, the FNTD and the tumor cells are scanned in a single step. Thus, the earliest cellular response irradiation and the spinels (indicated by black discs), acting as landmarks for later image registration are recorded. The initial stack typically comprises an image stack of ~ 30 imaging planes (2.). In a second step live-cell imaging comprising an image stack of ~3 imaging planes of the biological compartment (cell layer) is performed by widefield microscopy (3.) After imaging, the Cell-Fit-HD[4D] is transferred to confocal microscopy to read out the FNTD. Using image registration routines, each ion track (red arrows) can be reconstructed into the cell layer recorded in the initial readout. The tilt between cell layer plane and confocal planes indicates the separate acquisition on two different microscopes, followed by post-acquisition stitching and image registration. Figure and figure caption were taken from (Niklas et al., 2022).

The ion irradiation deposits the physical energy in the seeded cells via ions, whose trajectories later can be visualized and correlated with biologic readouts.

> *Note:* We describe the irradiation of Cell-Fit-HD[4D] which is aligned perpendicular to an incident horizontal carbon ion beam (Figure 3). In this protocol the cell layer was positioned in the middle of a 1 cm wide spread-out Bragg peak (SOBP) of carbon ions at a water equivalent depth of ~ 3.5 cm. Planned physical dose levels were 1 Gy and 0.5 Gy, respectively resulting in expected carbon ion beam fluences of $8.43 * 10^6$ cm^{-2} and $4.16 * 10^6$ cm^{-2}, respectively (Niklas et al., 2022). Our irradiation plan was similar to (Dokic et al., 2016).

The irradiation setup principally depends on beam-specific circumstances at the irradiation site and on the desired irradiation geometry. Start the heating of the microscope 2–4 h prior to irradiation to avoid spatial errors especially in the vertical dimension due to thermal expansion during imaging. Set up and save the imaging program prior to irradiation to minimize the interval between irradiation and imaging.

6. Prepare irradiation according to your planned physical dose level: position and potential stopping material (e.g., PMMA) to achieve desired linear energy transfer (LET) and desired ion beam fluence in the FNTD and in the cell layer. Shield the positions of control wells with additional stopping material.
7. Seal the Cell-Fit-HD[4D] plate in the laminar hood.

> *Note:* A switch to phenol-free medium at this point will markedly improve the signal-noise ratio in the red channel.

   a. Remove the plate lid and span a single piece of flexible wax-polyolefin film over the wells. Apply gentle pressure on the well edges.
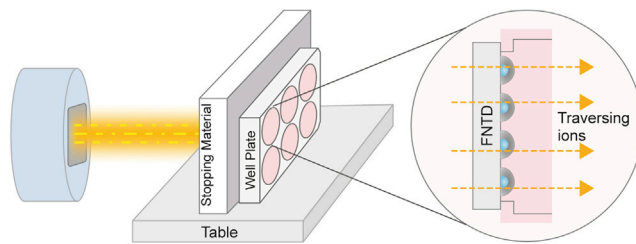
Figure 3. Exemplary irradiation setup for Cell-Fit-HD^{4D}
The biosensor is aligned perpendicular to the incoming ion beam. Additional stopping material in front of the well plate comprising the FNTD wafer coated with a single cell layer enables to locate the cell in the desired position of a Bragg peak. Figure and figure caption were taken from (Niklas et al., 2022). The irradiation setup was similar to (Dokic et al., 2016).

    b. Place a tissue with the approximate size of the plate on top of the wax sealing to maintain pressure during irradiation.

    c. Close the plate lid and seal the plate by wrapping the sides in flexible wax-polyolefin film while applying firm pressure to the lid.

    d. Incubate the Cell-Fit-HD^{4D} plate at cell culture conditions until irradiation.

8. Position the Cell-Fit-HD^{4D} plate perpendicular to the ion beam path, with the FNTD wafers in direct contact with the phantoms. Confirm sealing of the plate.

9. Start irradiation program. Here, a physical dose level of 1 Gy was delivered to Cell-Fit-HD^{4D} using a carbon ion beam. The biosensor was placed in the mid of SOBP and 3 cm of PMMA was used as stopping material in front of the biosensor.

Initial widefield image acquisition and live-cell microscopy

    ⏱ Timing: up to 5 days of live-cell imaging depending on experimental purpose.

The initial widefield image acquisition serves the rapid determination of the observed cell positions on the FNTD. Z-stacks of the FNTD as well as the superimposed cells allow for precise re-identification of imaged positions. Live-cell microscopy over the course of days enables long-term tracking of cellular responses.

10. Transfer the Cell-Fit-HD^{4D} plate to the widefield microscope as quickly as possible.

    ⚠ CRITICAL: While many molecular and cellular readouts might not require straightaway acquisition, the slight cell movements within minutes distort the spatial correlation of cells and ion tracks in the FNTD. As a consequence, the precision of dose deposition computation is negatively influenced by any delay between irradiation and initial acquisition.

11. Remove the sealing from the Cell-Fit-HD^{4D} plate and place it in the microscope stage. Apply the lid of a potentially associated micro incubator.

12. Start program. The number of recorded positions depend on the desired number of cells to be imaged. A recording of high number of positions will decrease precision in computation of physical energy deposition in the cells (see step 3 and paragraph limitations).

Fixation and immunofluorescent staining of cells (optional)

    ⏱ Timing: 20 min to 12 h (overnight) for fixation dependent on method, 6–24 h for staining depending on incubation time

Post-imaging staining provides the possibility to yield additional endpoint readouts of single imaged cells.

> *Note:* Avoid long exposure of the FNTD to bright light during the procedure.

13. Move the Cell-Fit-HD^{4D} plate from the microscope stage to a workbench and aspirate medium.
14. Wash 1× with PBS.
15. Apply fixation method of choice, mostly depending on which works best for the selected anti-bodies. Here, for staining of p21 using the listed antibody, EtOH-fixation was chosen, which occurs at −20°C overnight.
16. Wash 1× with PBS.
17. Apply blocking/ permeabilization buffer (1% Triton-X-100, 3% BSA in PBS) for 20 min at RT (room temperature).
18. Cover the FNTD wafer with sufficient volume of primary antibody diluted in washing buffer (blocking buffer 1:5 diluted in PBS, approximately 100 μL/well), and incubate overnight at 4°C. Alternatively, incubation at RT for 3–4 h might produce similar results.

> *Note:* To reduce required antibody solution volume and to circumvent capillary/ surface tension effects, consider covering the central growing area (=FNTD) with wax-polyolefin film for equal liquid distribution.

19. Wash 2× in washing buffer, 5 min incubation each.
20. Cover the FNTD wafer with secondary antibody diluted in washing buffer (blocking buffer 1:5 diluted in PBS, approximately 100 μL/well), and incubate 4–6 h at 4°C. Alternatively, incubation at RT for 1 h might produce similar results.

> *Note:* Applications of fluorophores with excitation and emission spectra in the near-far red region and beyond are recommended to avoid conflict with the FNTD emission spectrum or fluorescent proteins expressed by the cells when performing live-cell imaging with widefield microscopy. A short wavelength excitation of cells is still feasible if the FNTD is scanned prior to cell layer. For details see paragraph limitations.

21. Wash 1× in washing buffer, 5 min. Add DAPI or alternative nuclear dyes with longer emission wavelength such as DRAQ5 or phosphatinositol if desired. For details see paragraph limitations.
22. Wash 1× in PBS, 5 min.
23. Store in PBS at 4°C until imaging.

> *Note:* Reload previously imaged positions from the saved setup applied for time-lapse micro-scopy. Alternatively, yield staining signals after FNTD scan on the laser scanning microscope.

Readout of the FNTD

> ⏲ Timing: 2–16 h (overnight) dependent on number and dimension of the imaging areas, desired SNR which is affected by the ion beam quality.

The microscopy acquisition of the ion trajectories in the FNTD in form of track spot (radiochromic transformed color centers) recording enables the calculation of deposited energy patterns in single cells. Concurrent acquisition of spinels allows precise image registration on previously acquired widefield imaging of cells.

> *Note:* A detailed description of FNTD readout by CLSM including imaging parameters as well as image registration is presented in (Greilich et al., 2013; Niklas et al., 2016, 2022; Klimpki et al., 2016). The working distance of the objective should be compatible with the thickness

of the wafer. An oil objective should be favored to realize a numerical aperture (NA) which is close to the NA (1.76) of the FNTD. The FNTD can also be readout by widefield microscopy decreasing the readout time by a factor of 11 (Walsh et al., 2020). The SNR of the readout signal and its comparison to confocal readout data (up to now gold standard) is subject to current investigations.

24. Place the Cell-Fit-HD[4D] plate including PBS in case of cells to be imaged in the stage of the CLSM.
25. Locate the areas imaged in the initial readout.

    Note: It is recommended using the coordinate system of the microscope stage to note down the approximate positions of the well/ the FNTD which were imaged to speed up the process of re-finding them on the CLSM. Cells might be used to identify the scanned areas. Spinel constellations present unique landmarks to guarantee correct position scanning.

26. Scan the imaged area of the FNTD. Ensure that the entire imaging area acquired in the initial readout is covered. We used a 40× oil objective with sufficient field of view ($\sim$220 × 220 μm^2) in order to limit the number of tiles needed for the entire imaging area ($\sim$660 × 660 μm^2) in the initial readout. Make sure that the single imaging tiles have sufficient overlap (here: $\sim$20 μm) for subsequent stitching to gain the complete imaging field. The main imaging parameter in CLSM, namely laser power, dwell time and number of re-scans have to adjusted accordingly to gain sufficient signal-to-noise ratio. For subsequent analysis of the intensity distribution of the track spots and LET computation (see paragraph data processing: physical compartment) the measured count rate by the microscope's detection unit (here APDs) should be in a linear relationship to the expected count rate. The upper limit of the measured count rate is $\sim$5 MHz in our imaging setup. Hence a saturation of the detection unit is avoided. This is achieved by a limitation of the laser power, dwell time and number of re-scans. In case of increased detected count rates the APD saturation can be corrected by mathematical transformation prior to any quantitative analysis. For a detailed description we refer to (Greilich et al., 2013; Klimpki et al., 2016).

Readout of immunofluorescent staining of cells (optional)

⏱ Timing: 2 min to 1 h dependent on number and dimension of the imaging areas

Placing the stained cells on the previously utilized widefield microscope and reuse of the very same, saved positions of the time lapse microscopy allows for obtaining additional information of the irradiated and observed cells.

27. Scan the cell layer, if cells have been stained for additional biomolecules. Statistically relevant cell numbers are required for informative analyses. Recommended tile number to be scanned therefore is dependent on cell confluency. To allow a correlation of the recorded signal of additional biomolecules with the physical energy deposition in the object of interest (e.g., cell nucleus) positions have to be identical to the one of the recorded stacks in live-cell microscopy.

    △ CRITICAL: Imaging the cell layer with excitation wave length close to 405 nm prior to the FNTD readout can cause substantial bleaching and thus deletion of the detected ion traversals in the FNTD. This is not compatible with precise ion track reconstruction. For details see paragraph limitations.

Registration of ion trajectories to cells

⏱ Timing: dependent on the performance of the computer used for image processing and on the corresponding software

Registration of the images acquired via confocal microscopy (FNTD, ion tracks) to the ones obtained in the initial stack by widefield microscopy (cells) enables the precise determination of energies deposited in single cells.

> Note: We outline the ion track reconstruction in the cell nuclei - our target of interest. The entire data processing including stitching and registration of the data sets gained by the FNTD readout as well as by the initial readout is described in detail in (Niklas et al., 2016, 2022). For the principle of ion track reconstruction using the FNTD readout signal see (Niklas et al., 2013a; Klimpki et al., 2016). A detailed description of the cell tracking software LevelSet Tracker in Matlab for nucleus segmentation and -tracking can be found in (Dzyubachyk et al., 2010). In principal each tracking software can be used. For the image processing, including linear regression analysis each dedicated software like R (RStudio Team, 2020) or Matlab can be used. Fundamental algorithms we developed for the registration of ion trajectories to cells were uploaded on Mendeley Data (see key resources table).

Data processing: Biological compartment

Analysis of imaged cells includes segmentation and tracking, as well as registration of mitotic events and DNA damage/ RIF. This enables the correlation of molecular and cellular responses with respectively deposited energies days after irradiation on the single cell level.

28. Combine the data sets of the cell layer acquired in the initial readout and subsequent live-cell imaging. We performed maximum intensity z projections of the acquired image stack for each time point. Segment and track cells/ cell nuclei using *LevelSet Tracker* or other tracking algorithms which register mitotic events to gain time series of the black white (BW) masks of the cross-sectional areas of the tracked objects. Export single frame images to a distinct folder designated for each single cell.

   ⚠ CRITICAL: Precise segmentation of the nuclei in the initial readout is crucial for correct ion track-cell-assignment. Manually control cell masks and adjust tracking algorithm parameters if necessary.

   > Note: Long-term cell fate tracking can be conducted manually/ user-guided, or automatically, and any suitable program for automatic cell tracking can principally be utilized. We applied an algorithm which recognizes the topological changes of mitotic cells to follow up cell progenies (Dzyubachyk et al., 2010), which was complemented by user-guided control and correction for high cell densities. We tracked cells based on the pan-nuclear signal of the 53BP1-mCherry fusion protein (Dimitrova et al., 2008). Tracking algorithms and parameters need adjustment according to the respective cell signals.

29. Analyze RIF for single cells over time. Here, RIF number, size, and signal intensity was quantified.

   > Note: While we used trainable WEKA segmentation for ImageJ (Arganda-Carreras et al., 2017), any approach for RIF segmentation and measurement based on single cell, single frame images can be applied including macro scripts, machine learning, and neural networks. Other or additional live-cell readouts can be analyzed. Extra-nuclear readout signals require cell-based instead of nuclear-based segmentation, which e.g., can be achieved using transmitted light channel.

30. Apply the cell mask of the last scanned time-lapse frame on the post-time-lapse staining (if performed) channel and measure respective signal. Here, nuclear p21 signal was quantified and correlated with initially deposited energies to determine potential energy-dependent growth arrest (Figure 4).
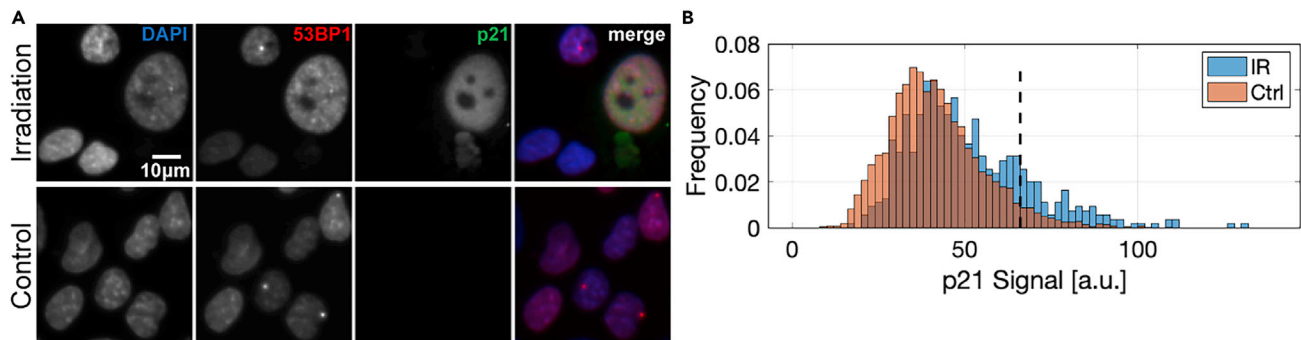
Figure 4. Fluorescent readout signal of the cell layer

(A) Representative fluorescent images of the cell cycle inhibitor p21, 53BP1 and DAPI. Cell-Fit-HD[4D] allows to identify p21 induction in a subpopulation of cells in response to irradiation.

(B) Histogram of p21 mean intensities in single cell nuclei (IR: C-12 irradiation 1 Gy, spread-out Bragg peak, Ctrl: control) including thresholding (66 a.u.) for p21-positive cells. Figure and figure caption were taken from (Niklas et al., 2022).

Data processing: Physical compartment

The recorded track spots are used for ion track reconstruction in the FNTD and extrapolation into the cell layer. Extrapolated ion tracks are assigned to cell nuclei. The intensity of the track spots is used to compute the energy deposition in individual cell nucleus.

31. Perform stitching of the recorded FNTD data sets according to (Niklas et al., 2016) to gain a single data set simplifying subsequent ion track reconstruction.

    Note: Here, a single imaging field of $\sim 660 \times 660 \ \mu m^2$ recorded in the initial readout with widefield microscopy using a 20× objective requires 4 × 4 confocal tiles using a 40× objective to ensure a complete coverage. An overlap of ~20 μm of the single tiles was used to ensure high accuracy in the stitching procedure. It is important to test for optical aberrations of the applied objectives and to limit them (e.g., by reducing the imaging field) to gain a stitching of high accuracy. Principally, all these read-out parameters depend on the specifications of the utilized microscope.

32. Use the in-house software *FNTD package* (Kouwenberg et al., 2016), a plugin for the *ImageJ/ Fiji* software (Arganda-Carreras et al., 2017) to identify and to link the track spots for subsequent reconstruction of the ion tracks in the FTND.

33. Perform linear regression analysis to fit the ion trajectory into a line based on the linked track spots. Use the slopes of the trajectory in both xz and yz directions to extrapolate the ion trajectories into the cell layer.

    Note: By applying maximum intensity z projections we reduced the dimensionality of the cell layer from 3D to 2D. To account for this reduction we extrapolated the ion tracks into the center of the cell layer in the vertical position of e.g., 2 μm (implying a thickness of cell layer $\sim 4 \ \mu m$) with respect to the FNTD surface.

34. To assess the number of ion traversals in each cell nucleus apply image registration of the data sets gained by widefield (cell layer) and confocal (FNTD) microscopy (step 3 in Figure 2). Calculate the intersection of the extrapolated ion trajectories with the BW masks of the cell nuclei (a logical AND operation) in the very first time point after irradiation, i.e., the initial readout.

35. For the calculation of the ions LET and deposited dose in the cell nucleus or object of interest we refer to (Rahmanian et al., 2017; Greilich et al., 2018; Niklas et al., 2022). Briefly, the track
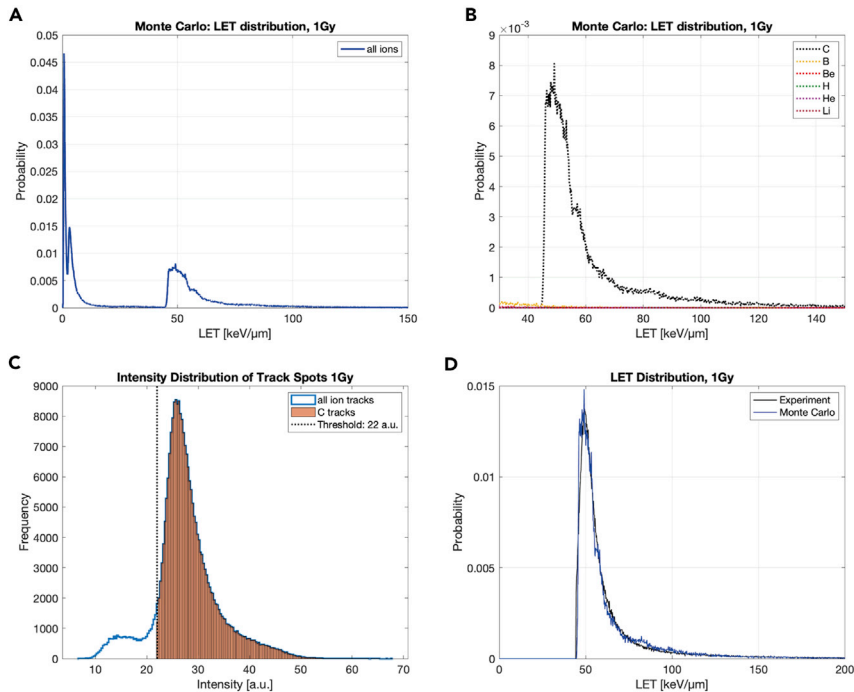
Figure 5. Exemplary intensity-to-LET conversion

(A) The LET-distribution by Monte Carlo simulation considering all ion types in the spread-out-Bragg peak (SOBP) of a carbon ion beam of 1 Gy is shown. The peak at 50 keV/μm correspond mainly to primary ions (carbon ions), the other peaks correspond to fragments.

(B) The individual distributions (carbon ions: C, fragments: B, Be, H, He, Li) constituting the peak at 50 keV/μm are depicted. The carbon ions dominate.

(C) Intensity distribution of ion traversals detected by the FNTD is shown. Intensity-based thresholding was applied to distinguish between primary ions (carbon ions, C) and fragments.

(D) Only the carbon ions (Experiment) were considered in the in the LET calculation. The intensity distribution of the carbon ions were mathematically transferred by $LET_j = 10^{\frac{1}{a}} - b$ to match the peak at 50 keV/μm in the LET distribution in (A) with I: track intensity of the ion, LETj: LET of the ion j, a and b: parameters adjusted to match intensity- and LET distribution. According to this transfer the intensity values were converted into LET values. For detailed description we refer to (Klimpki et al., 2016; Rahmanian et al., 2017; Greilich et al., 2018; Niklas et al., 2022).

spot intensity allows for computation of the LET of the corresponding ion. This is done by matching the intensity distribution of the detected track spots with a Monte Carlo generated LET distribution of the applied irradiation setup (Figure 5). For the ion beam fluence calculation the number of ion hits intersecting the BW mask of a cell nucleus/ object of interest are counted.

Note: The entire assessment of the physical energy deposition is based on the hit statistics gained in the previous step. In contrast to a simplified projection of the ions into the BW mask of a nucleus, an ion track reconstruction considering the incident angle of the ion is increasing the accuracy in dose calculation.

Data processing: Combination of physical and biological compartment

Physical beam parameters are correlated to biological readout parameters to resolve the cell's individual response chain triggered by the physical energy deposition in its nucleus.

36. Fuse the data on energy deposition and molecular dynamics/ gene expression/ cellular fate.
37. Correlate biological readouts to physical beam parameters.

EXPECTED OUTCOMES

Figure 6 and Methods video S2 illustrate the combination of acquired biological response data sets with the ion hit statistics computed for each cell nucleus after carbon ion irradiation of 1 Gy physical dose using a 1 cm wide spread-out Bragg peak (SOBP). The cell layer was positioned in the middle of the SOBP. Based on the live-cell imaging, subsequent cell tracking (identified cell nuclei are colorfully encircled in Figures 6A and 6B) and RIF extraction, a set of biological parameters of interest is extracted and assigned to each cell nucleus. We exemplarily show number of RIFs at different time points and the p21 status. Each cell nucleus identified in the first time point T_0 after irradiation gets a unique identification, termed *MotherID*. This identification further allows to link the parameter sets extracted from the daughter cells (with identification *DaughterID*) with the corresponding mother cell in the first time point.

By the ion track reconstruction, each nucleus of identification *MotherID* is assigned a set of ion hits and the corresponding LETs (Figure 6C). Based on this hit statistics further beam parameters, e.g., dose or $\sum$LET (sum of single ions LET in a cell nucleus) can be assigned to the cell nuclei. The identification *MotherID* is finally used to link the physical beam parameters with the extracted cellular response parameters for each irradiated and identified cell nucleus (Figure 6D).

The recording of individual cellular response dynamics and computation of the individual physical energy deposition allows for unique spatio-temporal correlation and combinations of physical and biological readout parameters on various time scales (Figure 6D). We demonstrated the correlation and linear regression analysis of RIF numbers in a cell nucleus 5.6 h after irradiation with the number of intranuclear carbon ion hits. Further, we exemplarily illustrated the possibility to track the proliferative fate of single cells in response to their distinctly received ion hit patterns. The cell tracking tool *LevelSet Tracker* applied here registers mitotic events based on nuclear changes in morphology during time lapse image series, and enables the construction of a directory including progeny as well as origin of each single cell over time. Hence, cell tracking and additional endpoint staining such as p21 allow for construction of cell division trees depicting initially irradiated cells, their progeny, and their cellular phenotype in terms of cell cycle arrest and the time point of time lapse run completion.

To draw a conclusion the readouts of Cell-Fit-HD[4D] allow to start resolving the cell's individual response chain triggered by the physical energy deposition in its nucleus after clinical ion beam irradiation.

LIMITATIONS

Particle irradiation and track resolution

The application of the Cell-Fit-HD[4D] protocol is at present probably mostly restricted by the accessibility to an ion radiation facility. The FNTD can principally detect the entire spectrum of primary ions and fragments at energies found in ion-beam cancer therapy (Osinga et al., 2013). In order to detect the entire ion spectrum in a complex irradiation field, i.e., high-LET primary ions (e.g., carbon ions) as well as very fast protons (fragments), a single readout of the FNTD can be time-consuming. The main readout parameters in confocal microscopy, namely laser power, dwell time and number of re-scans have to be adjusted accordingly. Multiple, sequential readouts of identical imaging field concentrating on the primary ions in a first step and on the fragments in a second step could be performed to circumvent this limitation. It yet has to be emphasized that the 94% of the energy is deposit by the primary ions in a carbon ion field. Hence the ion traversals by the primary ions dominate (and not the very fast fragments).

Imaging limitations

Fluorophores in the cell layer with excitation spectra near 450 nm (e.g., DAPI) should in principally be avoided. Excitation of such fluorophores would cause a radiochromic transformation of pristine F_2^{2+}(2Mg) color centers in the FNTD. This transformation is the principle mechanism behind the single ion detection (Akselrod and Kouwenberg, 2018). The application of such fluorophores would result in a deterioration of the intensity profile of the track spots - the ions characteristic signature left
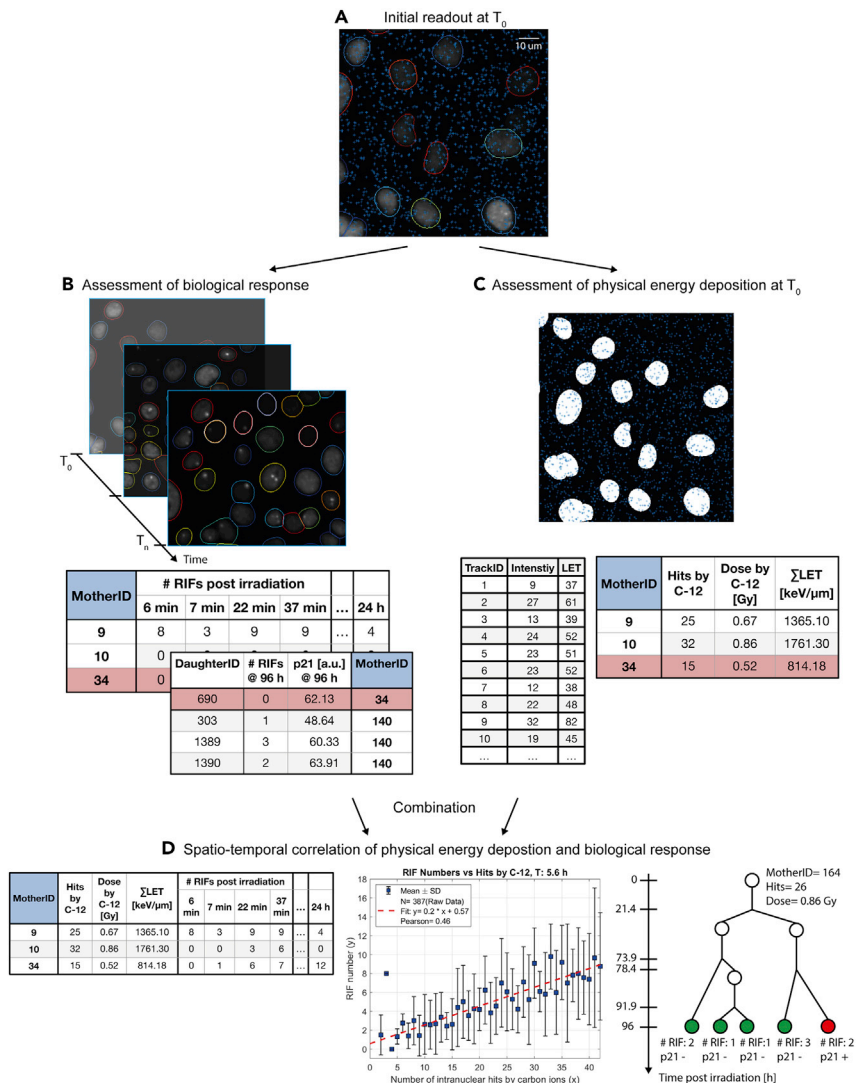
Figure 6. Spatio-temporal correlation of physical energy deposition in individual cell nuclei with cellular response

(A) Ion tracks (blue crosses) are reconstructed into the cell layer in the very first time point (T_0) after irradiation. The corresponding processed data sets were recorded in the initial readout. Cell nuclei were identified by cell tracking software.

(B) Cell nucleus tracking and radiation induced DNA damage foci (RIF) segmentation of the data set gained by live-cell imaging allows to assign each mother cell (identification: MotherID) and their corresponding daughter cells (identification: DaugherID) a set of biological parameters. In our case radiation induced foci (RIF) of the mother cell within 24 h after irradiation, number of RIFs and p21 level in the daughter cells at 96 h after irradiation.

(C) The ion traversals are reconstructed into a binary mask of the maximum intensity z projections gained by the initial readout. By assessment of the track intensity and hence LET (keV/µm) of individual ion traversal identified by TrackID, a set of physical beam parameters ($\sum$LET: sum of single ions LET in a cell nucleus) can be extracted for individual cell nucleus.

(D) Combining the biological and physical data sets generates unique spatiotemporal correlation of the energy deposition in a cell nucleus and its response. Exemplarily correlations, i.e., correlation of RIF numbers 5.6 h after irradiation with number of carbon ion hits in the corresponding nucleus as well as cell division tree are depicted. SD: standard deviation, RIF: radiation induced DNA damage foci.

in the FNTD - and thus would interfere the ion track reconstruction. A short wavelength excitation of cells is still feasible if the FNTD is scanned prior to cell layer. In contrast to widefield microscopy, the utilization of laser lines of short wavelength to excite fluorophores in the cell layer by confocal microscopy would only deteriorate the information on the track spots stored in the axial region of the FNTD close to the FNTD-cell interface. A reconstruction of the ion traversals is still possible but

of decreased accuracy (Niklas et al., 2013a). The pristine F_2^{2+}(2Mg) color centers can also be excited (but not radiochromic transformed) with green laser light, emitting fluorescent light centered at 520 nm. An excitation of such fluorophores in the cell layer with green laser light would cause disturbing background signal originating from the FNTD. Applying confocal microscopy with tight optical sectioning in axial direction could reduce this background.

Analysis limitations

In terms of the biological aspect, the observation time is confined by the proliferation of cells and the herewith linked increase in cell density and automatic cell tracking errors. Novel approaches and improvements for cell tracking algorithms bear the potential to overcome such limitation.

Uncertainties and inaccuracies result from inherent conditions of the utilized devices and procedures. Potential sources of errors affecting the computed physical energy deposition in the cell layer are:

Segmentation error of the cell nuclei applying a cell tracking routine,

Cell migration on the wafer in the time interval between irradiation and initial readout,

Error in registration procedure including stitching of single imaging tiles,

Uncertainty of the correct vertical position of the cell layer,

Uncertainty in track reconstruction expressed by the prediction interval.

The assessed mean error is ≤ 1.5 μm when taking the errors in registration procedure, uncertainties in the vertical position and in ion track reconstruction into account. This is yet much smaller than the dimension of a single cell nucleus of diameter 10 μm. As long as sufficient number of data points are available and systematic errors are avoided, an over- and underestimation of the assessed physical energy deposition in the nucleus should be in balance. We also developed a Monte Carlo-based simulation for the estimation of the total error in the number of ion hits in a cell nucleus. A detailed description on the assessed mean error and on the Monte Carlo-based simulation is given in (Niklas et al., 2022).

Spatial correlation of ion trajectories and subcellular responses

Spatial correlation of molecular damage to single ion traversals requires low ion beam fluences (Niklas et al., 2013c). Due to cellular- as well as chromatin movement and the delay in protein complex formation around DSB, exact spatial overlap of RIF and ion track in the FNTD cannot be expected. We also expect a significant risk of false correlation applying a dose level of 1 Gy in a carbon ion field (SOBP) with 27 (median) ion hits in a cell nucleus (Niklas et al., 2022). Recently presented correlations of ion trajectories and DSBs relied on direct fixation of cells following irradiation (Konishi et al., 2007; Kodaira et al., 2015; Niklas et al., 2013b) or deployed low ion beam fluences on single living cells under observation (McFadden et al., 2016). Both methods do not allow for long-term observation and fate tracking of a larger number of cells under clinically relevant physical dose levels of approximately 1 Gy. Nearest neighbor analysis including fingerprint analysis could improve spatial correlation analysis of single ion traversals and molecular response applying clinically relevant dose levels.

Economy

The price per FNTD depends on its shape and diameter. It is less than 200 USD for a round wafer of 11 mm diameter. The biosensor can be disassembled after the experiment and the wafer can be bleached and sterilized. All information on the ion traversals are lost and the wafer can thus be reused for another experiment.

TROUBLESHOOTING

Problem 1

Cells are not viable on the FNTD or show irregular morphology (step 2; Figure 1).

Potential solution

Both problems are most likely interconnected as irregular morphology indicates physiological stress, the result of which is growth arrest or cell death. This is probably caused by contact of cell culture medium with excessive or smeared tissue glue. Tissue residues which are visible within the well prior to cell seeding are unlikely to be successfully removed by washing. Consider waiving the construction and start over. Avoid lateral movement of the FNTD once it is contact with the plate bottom and consider reduction of deployed tissue volumes.

Problem 2

Cells do not attach to the FNTD (step 2).

Potential solution

Again, this could be a result of cell stress and cell death. However, some cell lines are more likely to attach to distinct materials than others. Coating the FNTD with commonly used compounds such as poly-lysine, gelatin or collagen should not be critical, unless it introduces distance of FNTD and cell layer. Non-direct contact of cells to the FNTD will require precise extrapolation of ion trajectories and thus exact determination of the coatings thickness. Alternatively, the mounting constriction might be considered in which case cells attach to the glass bottom, but which again requires extrapolation of ion trajectories.

Problem 3

Escaping fluid from wells (step 1; step 6–10).

Potential solution

Guarantee complete sealing and fluid retention by respectively long test incubation – optimally overnight - of the Cell-Fit-HD^{4D} plate on an underlying sheet of paper towel. Leaks might be fixed by additional application of minimal tissue glue volumes on the outer well bottom. Additional tools for leak fixation like silicon rings are not recommended due to potential interference with the microscope objective, but might be tested and confirmed for compatibility. Again, the alternative mounting architecture of Cell-Fit-HD^{4D} circumvents this potential problem by leaving the well bottom untouched.

Problem 4

Cells display non-physiological morphology and/ or behavior in the course of live-cell microscopy (step 12).

Potential solution

Poor performance of cells during live-cell microscopy can result from various aspects, most likely of which are suboptimal environmental conditions and phototoxicity.

Automatic regulation of temperature, humidity, and CO_2 is highly recommended and most definitely raises chances for experimental success. It is favorable to apply an additional thermometer sensor to a medium containing dummy well during the imaging course for feedback regulation of the heating system.

Phototoxicity can be reduced by decreasing channel number, single channel exposure times, number of imaged positions and imaged z-stack layers, as well as increase of scanning intervals. In general, a high-speed synchronization device which optimally orchestrates shutter and camera substantially decreases the exposure of cells to light.

Besides its acute toxic effects, residual tissue glue can induce milder, long term stress which negatively influences cell physiology and viability.

Last, the choice of culture medium influences cell physiology. If special imaging medium which lacks autofluorescent components like phenol-red is used, assure that it contains the required concentrations of metabolites like pyruvate or L-Glutamine. Consider running a control with the recommended full medium.

Problem 5
Photobleaching is observed during live-cell microscopy (step 12).

Potential solution
Fluorophore bleaching presents a severe problem for quantitative analysis which post-might not easily be corrected for. The effect can be diminished by the same means as for phototoxicity. Stable fluorescent protein transduction is recommended over transient live-cell staining to maintain robust fluorescent signals. Transiently staining compounds might be refreshed within the time-lapse microscopy setting, that is, without moving the plate.

Problem 6
Erroneous cell- and cell division tracking (step 29).

Potential solution
Precise cell tracking presents a delicate matter, especially in case of dividing and locomotive populations. Working with non-or low frequently dividing cells will substantially ease cell fate tracking. The risk for false cell assignment over time is reduced with low cell density, while cell movement, and to lower extent cell division, are usually retrenched in confluent 2D cultures. False cell assignment due to excessive cell movement, but also mitosis, can be counteracted by increase of scan frequency. Test different tracking algorithms or adjust parameters of tracking algorithms to fit the nature of the respective signals. For critical image sequences of dense, moving, and dividing cells, consider user-guided cell tracking or control of automatic tracking results.

RESOURCE AVAILABILITY

Lead contact
Further information and requests for resources and reagents should be directed to and will be fulfilled by the lead contact, Dr. Julian Schlegel (j.schlegel@dkfz.de).

Materials availability
All materials and constructs used in this study are maintained by Prof. Dr. Dr. Abdollahi's laboratory and are available upon request.

This study did not generate new unique reagents.

There are restrictions to the availability of FNTDs due to commercial distribution by the manufacturer.

Data and code availability
All data reported in this paper will be shared by the lead contact upon request.

All fundamental code applied for data generation reported in this paper is available online (https://doi.org/10.17632/cdt269pw7m.1). Additional requested code will be shared by the lead contact upon request.

Original/ source data for Figures 1–3 in the paper is available at (Niklas et al., 2022).

Any additional information required to reanalyze the data reported in this paper is available from the lead contact upon request.

SUPPLEMENTAL INFORMATION

Supplemental information can be found online at https://doi.org/10.1016/j.xpro.2022.101798.

AUTHOR CONTRIBUTIONS

J.S. and M.N. wrote, reviewed, and edited the manuscript. M.N., J.S., and K.R. visualized the data. O.D. developed the cell tracking software and assisted in the cell tracking. A.A. initiated, conceptualized, and supervised the project. All authors edited the paper. All authors read and approved the final paper.

DECLARATION OF INTERESTS

The authors declare no competing interests.

REFERENCES

Akselrod, M., and Kouwenberg, J. (2018). Fluorescent nuclear track detectors - review of past, present and future of the technology. Radiat. Meas. *117*, 35–51. https://doi.org/10.1016/j.radmeas.2018.07.005.

Akselrod, M.S., and Sykora, G.J. (2011). Fluorescent nuclear track detector technology – a new way to do passive solid state dosimetry. Radiat. Meas. *46*, 1671–1679. https://doi.org/10.1016/j.radmeas.2011.06.018.

Arganda-Carreras, I., Kaynig, V., Rueden, C., Eliceiri, K.W., Schindelin, J., Cardona, A., and Sebastian Seung, H. (2017). Trainable Weka segmentation: a machine learning tool for microscopy pixel classification. Bioinformatics *33*, 2424–2426. https://doi.org/10.1093/bioinformatics/btx180.

Dimitrova, N., Chen, Y.C.M., Spector, D.L., and de Lange, T. (2008). 53BP1 promotes non-homologous end joining of telomeres by increasing chromatin mobility. Nature *456*, 524–528. https://doi.org/10.1038/nature07433.

Dokic, I., Mairani, A., Niklas, M., Zimmermann, F., Chaudhri, N., Krunic, D., Tessonnier, T., Ferrari, A., Parodi, K., Jäkel, O., et al. (2016). Next generation multi-scale biophysical characterization of high precision cancer particle radiotherapy using clinical proton, helium-carbon- and oxygen ion beams. Oncotarget *7*, 56676–56689. https://doi.org/10.18632/oncotarget.10996.

Dzyubachyk, O., van Cappellen, W.A., Essers, J., Niessen, W.J., and Meijering, E. (2010). Advanced level-set-based cell tracking in time-lapse fluorescence microscopy. IEEE Trans. Med. Imaging *29*, 852–867. https://doi.org/10.1109/TMI.2009.2038693.

Greilich, S., Jansen, J., Neuholz, A., Stadler, A., Mescher, H., and Klimpki, G. (2018). Evaluation of additional track parameters from fluorescent nuclear track detectors to determine the LET of individual ions. Radiat. Prot. Dosimetry *180*, 206–209. https://doi.org/10.1093/rpd/ncx228.

Greilich, S., Osinga, J.-M., Niklas, M., Lauer, F.M., Klimpki, G., Bestvater, F., Bartz, J.A., Akselrod, M.S., and Jäkel, O. (2013). Fluorescent nuclear track detectors as a tool for ion-beam therapy research. Radiat. Meas. *56*, 267–272. https://doi.org/10.1016/j.radmeas.2013.01.033.

Klimpki, G., Mescher, H., Akselrod, M.S., Jäkel, O., and Greilich, S. (2016). Fluence-based dosimetry of proton and heavier ion beams using single track detectors. Phys. Med. Biol. *61*, 1021–1040. https://doi.org/10.1088/0031-9155/61/3/1021.

Kodaira, S., Konishi, T., Kobayashi, A., Maeda, T., Ahmad, T.A.F.T., Yang, G., Akselrod, M.S., Furusawa, Y., and Uchihori, Y. (2015). Co-visualization of DNA damage and ion traversals in live mammalian cells using a fluorescent nuclear track detector. J. Radiat. Res. *56*, 360–365. https://doi.org/10.1093/jrr/rru091.

Konishi, T., Amemiya, K., Natsume, T., Takeyasu, A., Yasuda, N., Furusawa, Y., and Hieda, K. (2007). A new method for the simultaneous detection of mammalian cells and ion tracks on a surface of CR-39. J. Radiat. Res. *48*, 255–261. https://doi.org/10.1269/jrr.06078.

Kouwenberg, J.J.M., Ulrich, L., Jäkel, O., and Greilich, S. (2016). A 3D feature point tracking method for ion radiation. Phys. Med. Biol. *61*, 4088–4104. https://doi.org/10.1088/0031-9155/61/11/4088.

McFadden, C.H., Rahmanian, S., Flint, D.B., Bright, S.J., Yoon, D.S., O'Brien, D.J., Asaithamby, A., Abdollahi, A., Greilich, S., and Sawakuchi, G.O. (2020). Isolation of time-dependent DNA damage induced by energetic carbon ions and their fragments using fluorescent nuclear track detectors. Med. Phys. *47*, 272–281. https://doi.org/10.1002/mp.13897.

McFadden, C.H., Hallacy, T.M., Flint, D.B., Granville, D.A., Asaithamby, A., Sahoo, N., Akselrod, M.S., and Sawakuchi, G.O. (2016). Time-lapse monitoring of DNA damage colocalized with particle tracks in single living cells. Int. J. Radiat. Oncol. Biol. Phys. *96*, 221–227. https://doi.org/10.1016/j.ijrobp.2016.04.007.

Niklas, M., Schlegel, J., Liew, H., Zimmermann, F., Rein, K., Walsh, D.W.M., Dzyubachyk, O., Holland-Letz, T., Rahmanian, S., Greilich, S., et al. (2022). Biosensor for deconvolution of individual cell fate in response to ion beam irradiation. Cell Rep. Methods *2*, 100169. https://doi.org/10.1016/j.crmeth.2022.100169.

Niklas, M., Henrich, M., Jäkel, O., Engelhardt, J., Abdollahi, A., and Greilich, S. (2017). STED microscopy visualizes energy deposition of single ions in a solid state detector beyond diffraction. Phys. Med. Biol. *62*, N180–N190. https://doi.org/10.1088/1361-6560/aa5edc.

Niklas, M., Zimmermann, F., Schlegel, J., Schwager, C., Debus, J., Jäkel, O., Abdollahi, A., and Greilich, S. (2016). Registration procedure for spatial correlation of physical energy deposition of particle irradiation and cellular response utilizing cell-fluorescent ion track hybrid detectors. Phys. Med. Biol. *61*, N441–N460. https://doi.org/10.1088/0031-9155/61/17/N441.

Niklas, M., Bartz, J.A., Akselrod, M.S., Abollahi, A., Jäkel, O., and Greilich, S. (2013a). Ion track reconstruction in 3D using alumina-based fluorescent nuclear track detectors. Phys. Med. Biol. 58, N251–N266. https://doi.org/10.1088/0031-9155/58/18/N251.

Niklas, M., Abdollahi, A., Akselrod, M.S., Debus, J., Jäkel, O., and Greilich, S. (2013b). Subcellular spatial correlation of particle traversal and biological response in clinical ion beams. Int. J. Radiat. Oncol. Biol. Phys. 87, 1141–1147. https://doi.org/10.1016/j.ijrobp.2013.08.043.

Niklas, M., Greilich, S., Melzig, C., Akselrod, M.S., Debus, J., Jäkel, O., and Abdollahi, A. (2013c). Engineering cell-fluorescent ion track hybrid detectors. Radiat. Oncol. 8, 141. https://doi.org/10.1186/1748-717X-8-141.

Niklas, M., Melzig, C., Abdollahi, A., Bartz, J., Akselrod, M.S., Debus, J., Jäkel, O., and Greilich, S. (2013d). Spatial correlation between traversal and cellular response in ion radiotherapy - towards single track spectroscopy. Radiat. Meas. 56, 285–289. https://doi.org/10.1016/j.radmeas.2013.01.060.

Osinga, J.-M., Akselrod, M.S., Herrmann, R., Hable, V., Dollinger, G., Jäkel, O., and Greilich, S. (2013). High-accuracy fluence determination in ion beams using fluorescent nuclear track detectors. Radiat. Meas. 56, 294–298. https://doi.org/10.1016/j.radmeas.2013.01.035.

Rahmanian, S., Niklas, M., Abdollahi, A., Jäkel, O., and Greilich, S. (2017). Application of fluorescent nuclear track detectors for cellular dosimetry. Phys.

Med. Biol. 62, N2719–N2740. https://doi.org/10.1088/1361-6560/aa56b4.

RStudio Team (2020). RStudio: Integrated Development for R (RStudio, PBC). http://www.rstudio.com/.

Sykora, G.J., Akselrod, M.S., Benton, E.R., and Yasuda, N. (2008). Spectroscopic properties of novel fluorescent nuclear track detectors for high and low LET charged particles. Radiat. Meas. 43, 422–426. https://doi.org/10.1016/j.radmeas.2007.11.009.

Walsh, D.W.M., Liew, H., Schlegel, J., Mairani, A., Abdollahi, A., and Niklas, M. (2020). Carbon ion dosimetry on a fluorescent nuclear track detector using widefield microscopy. Phys. Med. Biol. 65, 21NT02. https://doi.org/10.1088/1361-6560/abb7c5.